Humboldt-Universität zu Berlin

Importance of the Coulomb truncation technique in GW calculations

Bachelor Thesis

in fulfillment of the requirements for the degree
Bachelor of Science (B. Sc.)

Humboldt-Universität zu Berlin
Mathematisch-Naturwissenschaftliche Fakultät
Institut für Physik
AG Theoretische Festkörperphysik

submitted by

Clara Wassner
wassnerc@physik.hu-berlin.de

supervised by

1. Prof. Dr. Dr.h.c. Claudia Draxl
2. Prof. Dr. Norbert Koch

October 11, 2018

Table of Contents

1 Introduction

Computational materials science aims at the determination of solid-state properties by means of simulations. It complements experimental research and provides estimations for quantities that are not accessible by experiment. Undesired impurities in the sample or the challenges in controlling external parameters can hinder a precise determination. By contrast, parameters such as the atomic structure or the position of an impurity can be chosen exactly within a computational simulation. The controllability of the investigated system and the parameter therein represents the major advantage of computational materials science over experiment. The success of computational materials science is based on advances in computer technology and the usage of *ab-initio* methods. Accurate material simulations require computing power that scales badly with the size of the system under consideration. Over the past decades, advances in computer technology enabled the simulation of larger and larger systems. Today, computational material science can deal with systems of realistic complexity. Within condensed matter physics, *ab-initio* methods provide a solution to computationally intractable problems, *e.g.* the crystal structure prediction. The state-of-the-art methods for investigating real materials are the density-functional theory and the many-body perturbation theory. Density-functional theory can predict electronic ground state properties with great accuracy. Properties of excited electronic states are described precisely by the equations of many-body perturbation theory. Approximations to these equations, such as the GW approach, predict properties related to excited electronic states remarkably well.

Solid state physics deals with many-electron systems in periodic potentials. The Bloch theorem states that the electronic wavefunction has the form of a propagating plane wave multiplied by a periodic function. This function exhibits the same periodicity as the potential of the system. Periodic boundary conditions are settled for a bulk of solid. These facts of solid-state theory make the usage of a plane-wave basis very convenient to represent the electronic wavefunction of the solid. In addition, the discrete representation of the involved functions in reciprocal space supports computational approaches. Generally, the periodicity of the investigated system needs to be taken into account when choosing the basis set. For example, a system periodic only in one dimension requires a basis set consisting of one-dimensional plane waves. The usage of a three-dimensional basis would not yield discrete functions in reciprocal space. This would produce problems in a computational approach. In principle, a different computational code has to be developed for every dimensionality which a studied system can have. But this is not practicable, since it would be associated with vast additional effort.

Thus, in codes using a plane-wave basis set, always the three-dimensional most general case is implemented. In order to apply such a code to systems periodic in less than three dimensions, a so-called *super-cell* [1] is set up. It contains the structure of interest and a vacuum region in the finite direction. Through the implemented three-dimensional boundary conditions, the super-cell is replicated in every direction. Hence, the studied system of lower dimensionality is replicated in the finite direction as well and its images are separated through a slab of vacuum. But spurious interactions between these artificial images can lead to different results than the actual low-dimensional system would yield. To prevent these artificial interactions, the system has to be "isolated" in the finite direction from its own images. This is realized by increasing the distance between the replica until the interaction among them

is neglectable. That way, also systems with lower dimensionality can be examined with an implemented three-dimensional basis. Within this *super-cell approach*, nonphysical results can be prevented when the used vacuum region in the super-cell is sufficiently large.

Unfortunately, the enlargement of the super-cell comes with an increase of computational costs. This is why the system size that can be studied within reasonable time is limited. For ground-state calculations within density-functional theory (DFT), the additional computational effort of calculations with large super-cells is nowadays affordable. Regarding calculations based on many-body perturbation theory, this is not the case. To annihilate spurious interaction between periodic replica, the required separations are considerably larger than in DFT-based calculations. The evaluation of non-local operators makes GW calculations using the super-cell technique with large vacuum regions often computationally intractable.

The *Coulomb truncation technique* offers a possibility to use smaller super-cells and to still prevent spurious interaction effects. The long-ranged Coulomb potential is set to zero along the finite direction at a particular distance from the charge so that the Coulomb potentials of charges from different super-cells do not overlap. Artificial images are then isolated from each other without having to enlarge the super-cell. Several approaches using this technique have been developed so far. It has been successfully applied *i.a.* to two-dimensional hexagonal GaN sheets [2], a linear H_2 chain[3], and the Mg atom [4].

Within this work, the Coulomb truncation technique is presented in detail, and expressions of the Coulomb-cutoff potential in reciprocal space are developed, following Reference [2]. The singularities of the Coulomb-cutoff potential at the point Γ are treated analytically by replacing the value of the potential at the singular point with the averaged value of the potential in the vicinity of the singularity. The truncation method and the averaged values have been implemented in the full-potential all-electron density-functional-theory package **exciting** [5]. To investigate the impact of the Coulomb-cutoff technique on GW calculations, the electronic structure of the molecule acetylene (zero-dimensional) and of the polyacetylene chain (one-dimensional) is calculated. The convergence behavior of quasiparticle energies as a function of the vacuum size is examined. Thereby, the reduction of computational costs in GW calculations provided by the Coulomb-cutoff technique is shown.

This work is organized as follows. A short introduction to density-functional theory and the GW approximation is presented in Section 2. Section 3 discusses the treatment of systems with lower dimensionality and represents the main subject investigated within this thesis. In Section 4, it is outlined how **exciting** solves the eigenvalue problem by introducing a suitable basis, and further implementation details are given. Application of the truncation technique and the obtained results are described in Section 5.

2 Theoretical background

The following chapter gives a short overview of some theoretical aspects used in numerical codes, which calculate properties of solids. Atomic units are used throughout this work.

2.1 Density Functional Theory

Density functional theory is nowadays the state-of-the-art method for studying ground-state properties of materials, such as structural properties. It is so successful *i.a.* due to its comparatively low computational costs. This allows a treatment of systems with more particles at a sufficient accuracy level than other *ab-initio* methods do. For instance, the *coupled cluster* method [6], widely used in quantum chemistry, allows a very accurate determination of physical properties but is limited to systems with only a few atoms. In principle, every property of a material is given by the many-body Hamiltonian and the Schrödinger equation. Its solutions lead to many-body wavefunctions where the expectation value of every observable can be obtained. The Born-Oppenheimer-approximation motivates to separate the ionic motion from the electronic one. One assumes, that the lighter electrons react immediately to a change of the nuclear configuration. Hence, they can be treated as moving in an external potential and the Hamiltonian of an interacting electronic system with N particles can be expressed as a sum of the kinetic energy operator $\hat{T}$, the external potential due to the nuclei $\hat{V}_{ext}$, and the electron-electron interaction $\hat{V}_{\mathrm{ee}}$.

$$\hat{H}_{\mathrm{elec}} = \hat{H} = \underbrace{-\frac{1}{2}\sum_{i}^{N}\nabla_i^2}_{\hat{T}} + \hat{V}_{ext} + \underbrace{\frac{1}{2}\sum_{i}^{N}\sum_{j\neq i}^{N}\frac{1}{|\mathbf{r}_i - \mathbf{r}_j|}}_{\hat{V}_{\mathrm{ee}}} \tag{1}$$

Given that already the storage of a many-body wavefunction causes problems [7, p.3], it is not only analytically, but also numerically impossible to solve the electronic many-body Schrödinger equation.

Density functional theory turns away from a description of the state by means of the many-body wavefunction $\Psi(\mathbf{r}_1, \mathbf{r}_2, \ldots, \mathbf{r}_N)$ with $3N$ coordinates. Instead it uses a description of the system's state by the electronic density, requiring only 3 coordinates. Of course, the description of an interacting-electron system requires the distinction between different spin densities $n_\uparrow(\mathbf{r})$ and $n_\downarrow(\mathbf{r})$, but only the description of a general spin-unpolarized density will be given within this framework. In the following, a short description of the important Hohenberg-Kohn-theorem will be given, which provides the theoretical basis for DFT. Furthermore it is depicted how an auxiliary system of non-interacting electrons can be used to calculate the ground-state density of the actual interacting-electron system.

2.1.1 Hohenberg-Kohn Theorem

The electronic Hamiltonian (1) differs for different systems with the same particle number only by the difference in the external potential. If Ψ_{GS} denotes the ground state of a particular external potential, then the ground-state density can be calculated as

$$n(\mathbf{r}) = \langle \Psi_{\mathrm{GS}} | \hat{n}(\mathbf{r}) | \Psi_{\mathrm{GS}} \rangle \tag{2}$$

where $\hat{n} = \sum_i^N \delta(\mathbf{r} - \mathbf{r}_i)$ is the density operator. From the Schrödinger equation one obtains the ground-state wavefunction and the ground-state density. Hence, it is clear that the ground-state density is a functional of the external potential $n[\, V_{\text{ext}}(\mathbf{r})\,]$. Hohenberg and Kohn showed in their groundbreaking work [8], that the reverse is also true. The external potential is a unique functional of the density $V_{\text{ext}}[n(\mathbf{r})]$ as well, apart from a trivial constant. This means, that every possible $n(\mathbf{r})$, which satisfies the particle-conservation constraint

$$\int n(\mathbf{r}) d\mathbf{r} = N \tag{3}$$

gives at most one $V_{\text{ext}}(\mathbf{r})$. Furthermore, the ground-state wavefunction and hence every observable represent a unique functional of the density. The energy functional of an interacting-electron system can be written in the formal form

$$E[n] = T[n] + V_{\text{ext}}[n] + V_{ee}[n] \tag{4}$$

where $T[n]$ and $V_{ee}[n]$ are the functionals of the kinetic energy and the electron-electron interaction, respectively. The functional of the external potential $V_{\text{ext}}[n]$ can be expressed as

$$V_{\text{ext}}[n] = \int V_{\text{ext}}(\mathbf{r}) n(\mathbf{r}) d\mathbf{r}. \tag{5}$$

A second important theoretical basis for DFT is the extension of the variational principle, which indicates that the energy has a minimum at the correct ground state Ψ_{GS}. Hohenberg and Kohn showed that the ground-state energy, which is a functional of the density, achieves its minimum for the correct ground-state density

$$E_{\text{GS}}[\, n(\mathbf{r})\,] \geq E_{\text{GS}}[\, n_{\text{GS}}(\mathbf{r})\,] \tag{6}$$

provided that condition (3) is satisfied by the accounted densities. More formally, (3) can be taken into account through the introduction of a Lagrange multiplier μ such that the variational principle can be expressed in a different way [9, p.12] as

$$\frac{\delta}{\delta n}\left\{ T[n] + V_{ee}[n] + \int V_{\text{ext}}(\mathbf{r}) n(\mathbf{r}) d\mathbf{r} - \mu \int n(\mathbf{r}) d\mathbf{r} \right\} = 0. \tag{7}$$

2.1.2 Kohn-Sham auxiliary system

In order to introduce an auxiliary system of independent electrons, as proposed by Kohn and Sham in [10], the energy functional (4) is reformulated to detach the parts of the functional, which are known explicitly.

$$E[n] = T_0[n] + E_H[n] + \int V_{\text{ext}}(\mathbf{r}) n(\mathbf{r}) d\mathbf{r} + E_{\text{xc}}[n] \tag{8}$$

Besides the functional for the external potential, also the functional for the Hartree energy is known

$$E_H[n] = \frac{1}{2} \iint \frac{n(\mathbf{r}) n(\mathbf{r}')}{|\mathbf{r} - \mathbf{r}'|} d\mathbf{r} d\mathbf{r}'. \tag{9}$$

$T_0[n]$ represents the kinetic-energy functional for a system of independent electrons, whose ground-state wavefunction is given by a Slater determinant. The last term in (8) denotes the exchange-correlation energy, which is defined as the difference between the kinetic energy of an interacting-electron system and the independent-particle system as well as the difference between the exact electron-electron interaction energy and the Hartree approximation.

$$E_{\text{xc}}[n] = T[n] - T_0[n] + V_{ee}[n] - E_H[n] \tag{10}$$

Hence, it follows that $E_{\text{xc}}[n]$ contains all contributions of exchange (reduction in the total energy due to antisymmetry of the electronic wavefunction) and correlation (difference in energy between the real interacting-electron system and the Hartree-Fock value).

Application of the variational principle on (8) yields the equation,

$$\frac{\delta T_0[n]}{\delta n(\mathbf{r})} + \underbrace{V_{\text{ext}}(\mathbf{r}) + V_H(\mathbf{r}) + V_{\text{xc}}(\mathbf{r})}_{V_{\text{KS}}(\mathbf{r},[n])} = \mu \tag{11}$$

respecting the condition (3) by introducing a Lagrange parameter μ. The potentials are the functional derivatives of the particular energy contributions with respect to the electron density. Equation (11) is valid for a general system of interacting electrons under an external potential. Exactly the same equation also describes a system of non-interacting electrons moving in an external potential $V_{\text{KS}}(\mathbf{r},[n])$. Therefore, an independent-electron system can be assumed, whose density can be obtained by solving the one-particle Schrödinger equation

$$\left(-\frac{1}{2}\nabla^2 + V_{\text{KS}}(\mathbf{r},[n])\right)\psi_i^{\text{KS}}(\mathbf{r}) = \epsilon_i^{\text{KS}}\psi_i^{\text{KS}}(\mathbf{r}) \tag{12}$$

and setting

$$n(\mathbf{r}) = \sum_i f_i |\psi_i^{\text{KS}}(\mathbf{r})|^2 \tag{13}$$

for the density, with f_i denoting the occupation number of the ith state. Equation (12) is the famous Kohn-Sham (KS) equation, which can only be solved self-consistently due to the interconnection between the Kohn-Sham potential $V_{\text{KS}}(\mathbf{r},[n])$ and the electron density. The self-consistent field cycle implemented in **exciting** is presented in Appendix B.

Following the Hohenberg-Kohn theorem, the density (13), obtained from the KS-equation for a non-interacting-electron gas, is the same for the original interacting-electron system moving in the external potential $V_{\text{ext}}(\mathbf{r})$. Thus it is, in principle, possible to determine the exact ground-state density of an inhomogeneous electron gas with the aid of the auxiliary system. Since every observable represents a functional of the ground-state density, every expectation value can then be calculated. Unfortunately, this is not entirely true, because the exact energy functional of the density is not known. In particular, it is the exchange-correlation energy whose exact shape is unknown, and this is where the KS-approach depends on approximations. One such approximation is presented in the subsequent section. Despite this shortcoming, the KS-approach is very successful in a large variety of ground-state calculations.

It is important to note that the KS-orbitals $\psi_i^{\text{KS}}(\mathbf{r})$ in general have no physical meaning. Only the highest occupied orbital can be interpreted as the ionization energy, provided the

exact exchange-correlation functional is used. Also, KS-orbitals do not represent an actual electronic orbital but are only an auxiliary system. This approach cannot be directly used when excited systems shall be described or band-gab values predicted.

2.1.3 Local Density Approximation

The Local Density Approximation (LDA) for the exchange-correlation energy has been already introduced in the original work of Kohn and Sham [10]. It assumes that the exchange-correlation energy per particle of the inhomogeneous electron gas is the same as in the homogeneous electron gas, that is $\epsilon_{\mathrm{xc}}^{\mathrm{LDA}} = \epsilon_{\mathrm{xc}}^{\mathrm{HEG}}$, which is a *function* of the electron density

$$E_{\mathrm{xc}}[n] = \int n(\mathbf{r})\epsilon_{\mathrm{xc}}(n(\mathbf{r}))d\mathbf{r}. \tag{14}$$

Kohn and Sham showed that this is exact for the two limiting cases of slowly varying densities and high densities. The system of a homogeneous electron gas has been the subject of many studies, so that the exact exchange-energy density is known

$$\epsilon_{\mathrm{x}}^{\mathrm{HEG}}(n(\mathbf{r})) = -\frac{3}{4\pi}\left(3\pi^2 n(\mathbf{r})\right)^{1/3}. \tag{15}$$

There is no exact analytic expression known for the correlation-energy density of the homogeneous electron gas. Nevertheless, a numerical solution has been elaborated by Ceperly and Alder [11], using Monte-Carlo techniques.

In spite of its relative simplicity, this approximation is very successful in calculating ground-state energies, molecular equilibrium distances, lattice parameters etc. and is widely used nowadays. One of the reasons why LDA performs so well compared with other, more complicated, exchange-correlation functionals, is that it obeys the sum rule for the exchange-correlation hole [12]. The exchange-correlation hole signifies the depletion of electronic charge around a particular electron due to the Pauli exclusion principle, and the Coulomb repulsion. The summation rule reflects the fact that, if an electron is definitely at a certain point, it is missing from the rest of the system [9, p.17]. Problems of the LDA arise *i.a.* from spurious self-interaction and from the fact that it does not take into account corrections to the exchange-correlation energy at a particular point due to close-by inhomogeneities of the electron density. Besides LDA, many other approximations for the exchange-correlation energy with different levels of sophistication exist. They are not discussed within this work since only LDA is considered in following DFT calculations.

2.2 Many-body perturbation theory: *GW* approximation

Exchange and correlation effects make it impossible to describe the wavefunction of a many-body system exactly by an auxiliary system of independent particles (mean-field approach). In order to predict not only ground-state properties, which are already accurately enough described by the DFT, a better description of exchange and correlation effects is necessary. The following short overview is based on Ref. [13].

Within the many-body perturbation theory (MBPT), the central variable is not the density $n(\mathbf{r})$ anymore, but the time-ordered single particle Green's function $G(\mathbf{r}t, \mathbf{r}'t')$[1]. This

[1] Hereafter simply referred to as Green's function

function describes the propagation of a particle in an N-particle system with ground state Ψ_0^N, created at the point $(\mathbf{r}', t')$, relative to the point $(\mathbf{r}, t)$. Hence, the Green's function can be defined using the particle annihilation $\hat{\psi}(\mathbf{r}t)$ and creation operator $\hat{\psi}^\dagger(\mathbf{r}t)$ as

$$G(\mathbf{r}t, \mathbf{r}'t') = -i \left\langle \Psi_0^N | \hat{\tau}[\hat{\psi}^\dagger(\mathbf{r}t)\hat{\psi}(\mathbf{r}'t')] | \Psi_0^N \right\rangle . \tag{16}$$

The time-ordering operator $\hat{\tau}$ rearranges its arguments in order of descending time arguments from left to right where for each pair permutation a factor (-1) is added. It allows to describe with Eq.(16) either a propagating electron $(t > t')$ or a propagating hole $(t < t')$. One should be aware of the difference between an additional hole in the system and the exchange-correlation hole, described in the previous chapter. MBPT aims to predict *i.a.* the outcome of a direct (inverse) photo emission experiment, so to calculate the excitation energies $\epsilon_i^{N-1} = E_0^N - E_i^{N-1}$ $(\epsilon_i^{N+1} = E_i^{N+1} - E_0^N)$. It can be seen with the frequency dependent Lehmann representation

$$G(\mathbf{r}, \mathbf{r}'; \omega) = \sum_i \frac{\psi_i^{N+1}(\mathbf{r})\psi_i^{N+1\,*}(\mathbf{r}')}{\omega - \epsilon^{N+1} + i\eta} + \sum_i \frac{\psi_i^{N-1}(\mathbf{r})\psi_i^{N-1\,*}(\mathbf{r}')}{\omega - \epsilon^{N-1} - i\eta} \tag{17}$$

that the Green's function has poles at the many-particle excitation energies $\epsilon_i^{N\pm1}$. The Lehmann representation can be obtained by exploiting the closure relation and the Fourier transformation. η signifies an infinitesimally small, positive, real number and the $\psi_i^{N\pm1}$ describe the projections

$$\psi_i^{N-1}(\mathbf{r}) = \langle \Psi_i^{N-1} | \hat{\psi}(\mathbf{r}) | \Psi_0 \rangle \qquad \text{and} \qquad \psi_i^{N+1}(\mathbf{r}) = \langle \Psi_0 | \hat{\psi}(\mathbf{r}) | \Psi_i^{N+1} \rangle. \tag{18}$$

The Green's function obeys the Dyson equation [14], which can be reformulated using the Lehmann representation of the Green's function. One obtains the non-linear quasiparticle equation

$$\left[-\frac{1}{2}\nabla^2 + \hat{V}_{\text{ext}} + \int \frac{n(\mathbf{r}')}{|\mathbf{r} - \mathbf{r}'|} d\mathbf{r}' \right] \psi_i^{N\pm1}(\mathbf{r}) + \int \Sigma(\mathbf{r}, \mathbf{r}'; \omega(\epsilon_i^{N\pm1}))\psi_i^{N\pm1}(\mathbf{r}')d\mathbf{r}' = \epsilon^{N\pm1}\psi_i^{N\pm1}(\mathbf{r}) \tag{19}$$

with the non-local, frequency-dependent and non-Hermitian self-energy operator $\Sigma(\mathbf{r}, \mathbf{r}'; \omega)$, containing all exchange and correlation effects that go beyond the Hartree potential V_H. The electron together with its interactions (induced by the other particles) can be called a quasiparticle. The exchange-correlation hole around the electron partially screens the charge of the electron such that the quasiparticles interact via a dynamically-screened interaction $W(\mathbf{r}, \mathbf{r}'; \omega)$

$$W(\mathbf{r}, \mathbf{r}'; \omega) = \int \epsilon^{-1}(\mathbf{r}, \mathbf{r}''; \omega) v(\mathbf{r}'', \mathbf{r}') d\mathbf{r}'' \tag{20}$$

where $\epsilon(\mathbf{r}, \mathbf{r}'; \omega)$ signifies the dielectric function and $v(\mathbf{r}, \mathbf{r}') = 1/|\mathbf{r} - \mathbf{r}'|$ the bare Coulomb potential.

The Hedin equations [15] provide a set of integral equations which link together different quantities such as the Green's function $G(\mathbf{r}, \mathbf{r}'; \omega)$, the self-energy $\Sigma(\mathbf{r}, \mathbf{r}'; \omega)$, the dynamically-screened interaction $W(\mathbf{r}, \mathbf{r}'; \omega)$, and the polarization function $P(\mathbf{r}, \mathbf{r}'; \omega)$. These equations

cannot be solved exactly, therefore a solution relies on approximations. A possible simplification provides the GW approximation. Within the GW approximation (GWA) the self-energy is assumed to be

$$\Sigma^{\mathrm{GW}}(\mathbf{r},\mathbf{r}';\omega) = \frac{i}{2\pi}\int_{-\infty}^{\infty} G_0(\mathbf{r},\mathbf{r}';\omega+\omega')W(\mathbf{r},\mathbf{r}';\omega')\exp^{i\omega'\eta}\,d\omega' \tag{21}$$

where G_0 is the Green's function of a system defined by the single-particle Hartree equation

$$\left[-\frac{1}{2}\nabla^2 + \hat{V}_{\mathrm{ext}} + \int \frac{n(\mathbf{r}')}{|\mathbf{r}-\mathbf{r}'|}d\mathbf{r}'\right]\varphi_i^0(\mathbf{r}) = \epsilon_i^0\varphi_i^0(\mathbf{r}). \tag{22}$$

For the Green's function G_0, the ψ_i^{N+1} and ψ_i^{N-1} in (17) denote the unoccupied and occupied states of a Hartree system, respectively. The GWA uses the random-phase approximation which gives for the dielectric and polarization function

$$\epsilon(\mathbf{r},\mathbf{r}';\omega) = \delta(\mathbf{r}-\mathbf{r}') - \int v(\mathbf{r},\mathbf{r}'')P(\mathbf{r}'',\mathbf{r}';\omega)d\mathbf{r}'' \tag{23}$$

$$P(\mathbf{r},\mathbf{r}';t-t') = -iG_0(\mathbf{r},\mathbf{r}',\tau)G_0(\mathbf{r}',\mathbf{r},-\tau) \tag{24}$$

where $\tau = t - t'$ is the Fourier transformation partner-variable of ω.

In order to obtain the excitation energies $\epsilon_i^{N\pm1}$, the quasiparticle equation (19) has to be solved. This is done by exploiting the similarity with the Kohn-Sham equation (12). Despite the missing physical justification, the Kohn-Sham energies ϵ_i^{KS} often estimate the band structure quite reasonably, which justifies a perturbative approach of first order

$$\epsilon_i^{N\pm1} \approx \epsilon_i^{\mathrm{KS}} + \left\langle\varphi_i^{\mathrm{KS}}|\Sigma(\epsilon_i^{N\pm1}) - V_{xc}|\varphi_i^{\mathrm{KS}}\right\rangle \tag{25}$$

since the correction to the exchange-correlation potential by the self-energy seems to be small. This perturbative approach is usually referred to as G_0W_0 in literature [7]. Equation (25) is non-linear in energy because of the energy dependence of the non-local self-energy. This can be further approximated by the linear expansion of the self-energy

$$\Sigma(\mathbf{r},\mathbf{r}';\epsilon_i^{N\pm1}) \approx \Sigma(\mathbf{r},\mathbf{r}';\epsilon_i^{\mathrm{KS}}) + (\epsilon_i^{N\pm1} - \epsilon_i^{\mathrm{KS}})\left.\frac{\partial\Sigma(\mathbf{r},\mathbf{r}';\omega)}{\partial\omega}\right|_{\omega=\epsilon_i^{\mathrm{KS}}} \tag{26}$$

which leads to

$$\epsilon_i^{N\pm1} \approx \epsilon_i^{\mathrm{KS}} + Z_i\left\langle\varphi_i^{\mathrm{KS}}|\Sigma(\epsilon_i^{\mathrm{KS}}) - V_{xc}|\varphi_i^{\mathrm{KS}}\right\rangle \tag{27}$$

where Z_i denotes the quasiparticle renormalization factor

$$Z_i = \left(1 - \left\langle\varphi_i^{\mathrm{KS}}\left|\left.\frac{\partial\Sigma(\mathbf{r},\mathbf{r}';\omega)}{\partial\omega}\right|_{\omega=\epsilon_i^{\mathrm{KS}}}\right|\varphi_i^{\mathrm{KS}}\right\rangle\right)^{-1}. \tag{28}$$

Thus, proceeding from a DFT calculation with KS-energies ϵ_i^{KS} and KS-eigenstates φ_i^{KS}, good approximations to the excitation energies like (27) can be obtained with the equations (20), (21), (23) and (24).

3 Simulation of systems with different dimensionality

The periodic structure of crystals leads to the Bloch theorem (62) (see Appendix A). For such a 3D(periodic)-system, plane waves offer a very convenient tool for representing the periodic functions. The Fourier transform is discrete, and several numerically efficient algorithms exist to perform the Fourier transformation *e.g.* FFT. However, not only the properties of 3D-systems but also the properties of systems with lower dimensionality, *e.g.* molecules, are of interest. To simulate a nD(periodic)-system, where $n = \{0, 1, 2\}$, one would require to use different basis functions for each case, in order to take into account the particular periodic dimensionality. In practice, the most general solution of 3D-periodic boundary conditions and the corresponding 3D Fourier transformation is used. Nevertheless, one wants to cover with one code as many applications as possible, regarding the range of properties and the variety of materials which can be studied. In order to enable also the study of systems with lower dimensionality than the implemented one, the super-cell technique [1] is applied. It allows to compute properties of lower-dimensional systems without changing completely all implemented procedures (*e.g.* from 3D Fourier transformation to 2D) and basis sets for every dimensionality, since this would be associated with vast additional effort. A super-cell is build up from the unit cell of the lower-dimensional system to which an additional vacuum region is added in the finite direction(s). Owing to the implemented periodic boundary conditions, the super-cell is replicated in every direction and artificial images of the lower-dimensional structure arise. In order to calculate, for example, the properties of a 2D-system (layer), the 3D-periodic boundary conditions lead to an infinite reproduction of the slab in the actually finite direction as well, see Figure 1. The simulated system then mimics a system of capacitors rather than an isolated layer. Due to the long-ranged Coulomb interaction between the particles, neighboring images can interact with each other. This leads to spurious effects in the finite directions for systems with lower dimensionality.

An easy solution so far was to choose the vacuum region large enough so that the potential generated by the particles, which decays with $\frac{1}{|\mathbf{r}|}$, is already sufficiently week at the border of the super-cell. The periodic images can thus be handled as not feeling each other. So it is clear that with increasing box size one can obtain more accurate results. On the other hand, the calculation time required to reach convergence increases rapidly with larger box sizes. This is because more basis functions for the expansion of the KS-wavefunctions are used (number of $\mathbf{G}$-vectors included) and thus the Hamiltonian to diagonalize is bigger. To compute the converged energy of the highest occupied molecular orbital (HOMO) of an isolated acetylene molecule, one has to use a box size of around 16 bohr (see Fig.3). This leads to a computational overhead (compared to the simulation of a periodic structure) due to exponential scaling. Figure 2 shows the exponential increase of calculation time needed to reach convergence of the ground-state energy of acetylene as a function of the box size.

For ground-state calculations, the required computational costs, unlike some decades ago, are nowadays affordable. This is not the case for calculations of excited properties e.g. GW calculations. The GW method is based on the explicit treatment of non-local operators in space and time. Such quantities, *e.g.* the dielectric function (23) or the self-energy (21), are long-ranged and force to use larger super-cells than a DFT calculation. Moreover, they are computationally also much more involved than DFT. Hence, larger box sizes are required to prevent spurious interactions among replica. Furthermore, an enlargement of the box size

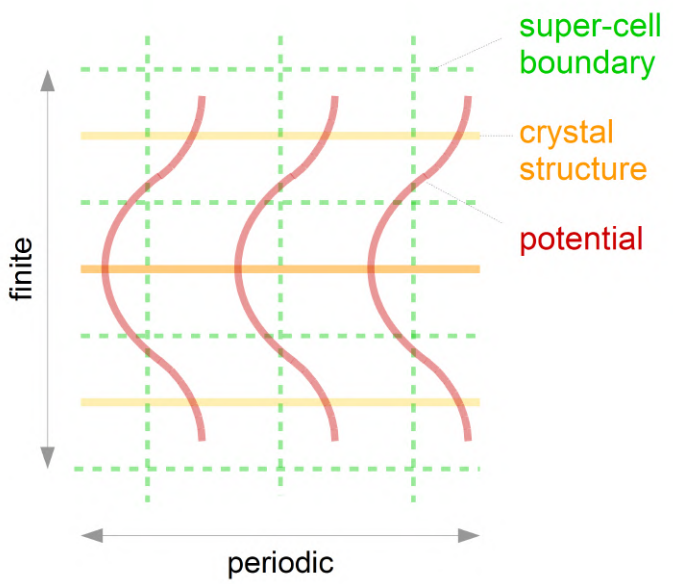

Figure 1: *A code such as* **`exciting`** *reproduces the object also in the finite direction(s) by using 3D-periodic boundary conditions and the super-cell approach. Hence, it simulates not directly the actual lower-dimensional system at hand. The figure exemplifies this for a 2D-system where the artificial interaction (red) between the replica leads to an observed system with properties similar to a capacitor rather than to that of the desired isolated layer (orange). For clarity, the second periodic direction has been omitted.*

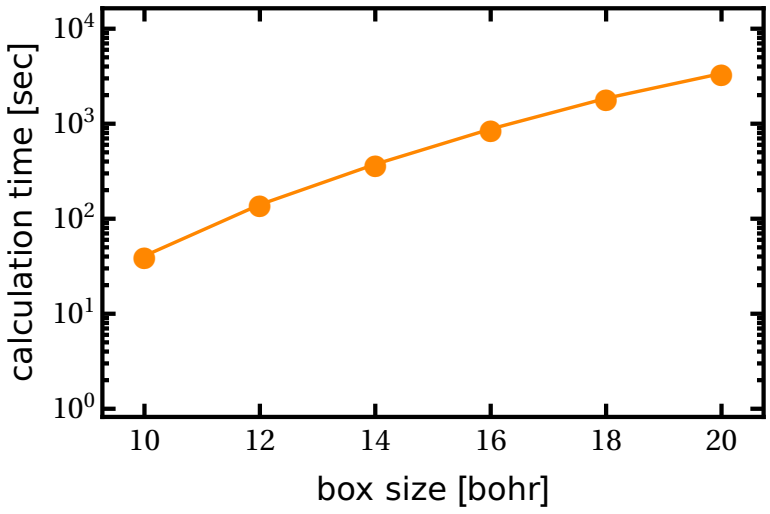

Figure 2: *Required calculation time to reach convergence of the ground-state energy of acetylene as a function of the box size (convergence criterion: change in energy between two iterations smaller than 10^{-6}). All calculations for the different box sizes were performed with the same parameter setting. The exponential dependency of computation time on box size becomes apparent.*

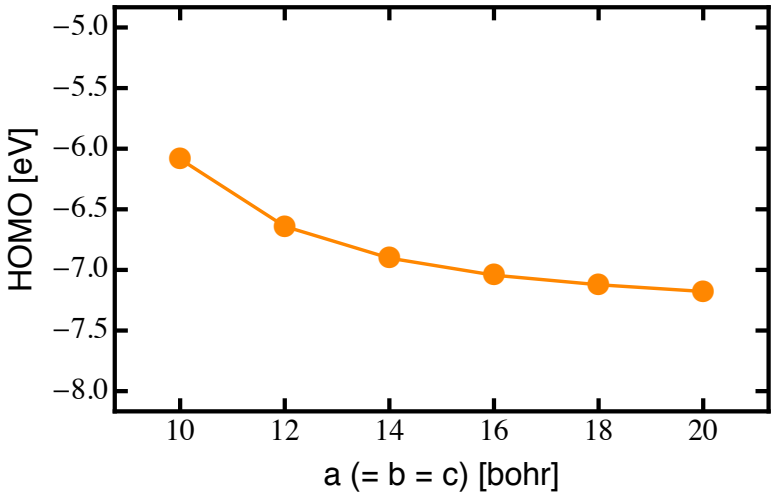

Figure 3: *Highest occupied molecular orbital (HOMO) of acetylene as a function of the box size, calculated with the DFT approach, using LDA. As can be seen, a converged energy value can be obtained with a box size of around 16 bohr.*

has a much larger impact on the computational costs in this case than in a ground-state calculation. This motivates different approaches to the artificial-image problem in order to save computational power.

3.1 Coulomb potential cutoff technique

A solution to the problem of artificial-image interaction is provided by the Coulomb-cutoff technique [2] [4] [3]. To avoid using large super-cells, the potential interaction is modified such that the potential equals the bare Coulomb potential inside some defined region D and zero outside [4].

$$v_c(\mathbf{r}) = \begin{cases} \frac{1}{|\mathbf{r}|} & \text{if } \mathbf{r} \in D \\ 0 & \text{if } \mathbf{r} \notin D \end{cases} \tag{29}$$

By truncating the potential, artificial interactions between replica can be prevented. This is desired only in the finite direction of the studied system, whereas the interaction between periodic cells has to be kept for periodic directions.

Since calculations of properties of solids require sums over the Brillouin zone ($\mathbf{k}$-point sampling) and/or reciprocal-lattice vectors, an expression for the Coulomb-cutoff potential (29) in the reciprocal space is needed. Therefore the Fourier transform

$$v_c(\mathbf{q}) = \int v_c(\mathbf{r}) \exp^{-\mathrm{i}\mathbf{q}\cdot\mathbf{r}} \mathrm{d}^3\mathbf{r} \tag{30}$$

has to be determined. Given that the truncation has to be performed only in the finite direction, Eq.(30) needs to be calculated for every n-periodic case separately ($n = 0, 1, 2, 3$) because every case requires a different region D.

In case of a zero-dimensional system (molecule, atom) the potential has to be truncated in every direction so region D is assumed to be spherical with radius R_c. The straight-forward calculation gives

$$v_c^{0\mathrm{D}}(\mathbf{q}) = \frac{4\pi}{\mathbf{q}^2}\left\{1 - \cos(qR_c)\right\} \tag{31}$$

where q denotes the absolute value of $\mathbf{q}$.

Systems, periodic in one dimension, require a two-dimensional region D. Without loss of generality the periodic direction is set along the z-axis of a Cartesian coordinate system. Performing the Fourier transformation in z-direction one obtains

$$v_c^{1\mathrm{D}}(\mathbf{q}) = \iint \mathrm{d}x\mathrm{d}y\, \Theta(x,y)\, 2\mathrm{K}_0(|q_z|\rho)\cos(q_x x + q_y y) \tag{32}$$

where $\rho = \sqrt{x^2+y^2}$ and $\mathrm{K}_0(z)$ indicates the modified Bessel function of the second kind. $\Theta(x,y)$ denotes a function which equals one inside a small region around the z-axis and zero elsewhere. The shape of $\Theta(x,y)$ will be specified later on.

For systems which extend infinitely in two dimensions, the truncation should be carried out only in one dimension. The finite direction is set to be along the z-axis and D extends in z-direction from $-z_c$ to z_c. The Fourier transformation gives

$$v_c^{2\mathrm{D}}(\mathbf{q}) = \frac{4\pi}{\mathbf{q}^2}\left\{1 + e^{-q_{xy}z_c}\left(\frac{q_z}{q_{xy}}\sin(q_z z_c) - \cos(q_z z_c)\right)\right\} \tag{33}$$

where $q_{xy} = \sqrt{q_x^2 + q_y^2}$.

For crystals, infinitely extended in every direction, the Coulomb potential does not have to be truncated. The Fourier transform of the Coulomb potential is given by the usual

$$v_c^{3\mathrm{D}}(\mathbf{q}) = \frac{4\pi}{\mathbf{q}^2} \tag{34}$$

3.2 Treatment of the $\mathbf{q} \to 0$ singularity

Expressions (31)-(34) exhibit divergences *i.a.* at the Γ-point. Since electronic properties are calculated by summations over the BZ (see Appendix A: Bloch Theorem and **k**-point sampling), this is a problem, given that the sums then become infinite. A simple exclusion of divergent points from the calculated sum over the BZ does not satisfy the demanded accuracy. This is due to the large contribution of the singularity's vicinity to the summation. Furthermore, a large drawback of avoiding using the Γ-point is a very slow convergence with respect to the **k**-point sampling of the BZ.

Since the GW implementation in **`exciting`** is based on Γ-point-centered grids, an explicit treatment of the $\mathbf{q} \to 0$ singularities is required. One possibility to do so is the idea of replacing the value at one **k**-point with the average value in a small volume around this point. Therewith it is also possible to take into account the large contribution of the singularity. It is hereafter referred to this procedure as the *method of averaging*. In order to treat the singularity at the Γ-point with the method of averaging, it is necessary, that Γ is an isolated singularity. This is not the case in Eqs.(32) and (33). By imposing special requirements on the cutoff region D [2], the singularities can be confined to the Γ-point only.

The different periodic cases are treated separately below by defining the cutoff region D, if necessary, and then treating the remaining singularity at Γ.

3.2.1 0D system

For the 0D case, there is no singularity. The value of $v_c^{0\mathrm{D}}(\mathbf{q})$ is finite for every value of $\mathbf{q}$ as can be seen with the following transformation, using the series expansion of the cosine.

$$v_c^{0\mathrm{D}}(\mathbf{q}) = \frac{4\pi}{q^2}\left\{1-\cos(qR_c)\right\} = -2\pi R_c^2 + \sum_{n=2}^{\infty}\frac{(-1)^n}{(2n)!}q^{2n-2}R_c^{2n} \tag{35}$$

Thus, the value of the 0D-cutoff potential at the Γ-point is

$$v_c^{0\mathrm{D}}(\mathbf{q}=0) = -2\pi R_c^2. \tag{36}$$

3.2.2 1D system

The Fourier transform of the 1D-cutoff potential (32) is in this form divergent in the whole q_xq_y-plane due to the singularity of the modified Bessel function of the second kind at the origin

$$\mathrm{K}_0(\chi\to 0) = -0.5772 + \ln(2) - \ln(\chi). \tag{37}$$

In order to reach a finite number of singularities, $\Theta(x,y)$ in Eq.(32) is defined so that $v_c^{1\mathrm{D}}(\mathbf{q})$ is set $\neq 0$ in exactly one Wigner-Seitz cell, which is centered on the wire in the xy-plane, as proposed in Ref.[2]

$$v_c^{1\mathrm{D}}(\mathbf{q}) = \iint_{\mathrm{WS}} 2\cdot\mathrm{K}_0(|q_z|\rho)\cdot\cos(q_xx+q_yy)\,dxdy. \tag{38}$$

Thus, the divergence is confined to the single term $\mathbf{q}=0$. This is due to the fact that the Brillouin zone is sampled with only one $\mathbf{k}$-point in the finite directions. Hence, every projection of a vector in the reciprocal space $\mathbf{q}$ on the q_xq_y-plane equals a reciprocal-lattice vector $\mathbf{G}$. The general relation [16] between a reciprocal-lattice vector $\mathbf{G}$ and a real-space-lattice vector $\mathbf{L}$

$$\mathbf{G}\cdot\mathbf{L} = 2\pi m \tag{39}$$

where m indicates an arbitrary integer, makes the xy-integral over the Wigner-Seitz cell disappear. This will be exemplarily shown for a rectangular Wigner-Seitz cell with side lengths L_x, L_y and L_z. First, the divergent term in (38) is isolated using (37)

$$-2\ln(|q_z|)\iint_{\mathrm{WS}}\cos(q_xx+q_yy)\,dxdy, \tag{40}$$

then the integration is performed and (39) is exploited

$$\begin{aligned}
\iint_{\mathrm{WS}}\cos(q_xx+q_yy)\,dxdy &= \int_{-L_x/2}^{L_x/2}\int_{-L_y/2}^{L_y/2}\cos(q_xx+q_yy)\,dydx\\
&= \frac{4}{q_xq_y}\sin(q_xL_x/2)\sin(q_yL_y/2)\\
&= \frac{4}{q_xq_y}\sin(\pi m)\sin(\pi m)\\
&= 0.
\end{aligned}$$

In order to treat the remaining divergence at $\mathbf{q} = 0$ with the method of averaging, the divergent term of (38) for $q_x = q_y = 0$ and $q_z \to 0$ is being extracted:

$$\begin{aligned} v_c^{1\mathrm{D}}(\mathbf{q} \to 0) &= \iint_{\mathrm{WS}} dxdy\, 2 \cdot (-0.5772 + \ln(2) - \ln(|q_z|\rho)) \\ &= \underbrace{-2 \cdot \ln(|q_z|) \cdot \Omega_{xy}}_{=:I^{1\mathrm{D}},\ \text{divergent for } q_z=0} \\ &\quad + \underbrace{2 \cdot \Omega_{xy} \cdot (-0.5772 + \ln(2)) - \iint_{\mathrm{WS}} \ln(x^2+y^2)dxdy}_{\text{constant for } q_z=0} \end{aligned} \tag{41}$$

$\Omega_{xy} := \iint_{\text{Wig-Sei}} dxdy$ represents the volume of the unit cell in the xy- plane. For the divergent term in (41), the average value over a small volume $V^{1\mathrm{D}}$ (in reciprocal space) around Γ is calculated. Because of the periodicity in only one direction, the Brillouin zone with volume Ω_{BZ} can be assumed as one-dimensional. Thus, $V^{1\mathrm{D}}$ represents a line in q_z-direction with length $\beta^{1\mathrm{D}} = \frac{\Omega_{BZ}}{N_{\mathbf{k}}} = V^{1\mathrm{D}}$, where $N_{\mathbf{k}}$ is the number of $\mathbf{q}$-points in a Brillouin zone. The divergent term can then be expressed as

$$\begin{aligned} I^{1\mathrm{D}} &= \frac{1}{V^{1\mathrm{D}}} \int_{V^{1\mathrm{D}}} dq_z\, (-2 \cdot \ln(|q_z|) \cdot \Omega_{xy}) \\ &= -\frac{2 \cdot \Omega_{xy}}{\beta^{1\mathrm{D}}} \int_{-\beta^{1\mathrm{D}}/2}^{\beta^{1\mathrm{D}}/2} dq_z\ \ln(|q_z|) \\ &= 2 \cdot \Omega_{xy} \cdot \left[\ln\left(\frac{\Omega_{BZ}}{2 \cdot N_{\mathbf{k}}} \right) - 1 \right]. \end{aligned} \tag{42}$$

Returning to the example of a rectangular Wigner-Seitz cell, the integral in the constant term of (41) gives

$$\begin{aligned} \iint_{\mathrm{WS}} \ln(x^2+y^2)dxdy &= \int_{-L_x/2}^{L_x/2} dx \int_{-L_y/2}^{L_y/2} dy\ \ln(x^2+y^2) \\ &= L_x \left((L_y\,(-3 - \ln(4) + \ln(L_x^2 + L_y^2)) + L_x\ \arctan\left(\frac{L_y}{L_x}\right) \right) \\ &\quad + L_y^2\, \mathrm{arccot}\left(\frac{L_y}{L_x}\right). \end{aligned}$$

The value of the 1D-cutoff potential at the Γ-point for an arbitrary Wigner-Seitz cell is

$$v_c^{1\mathrm{D}}(\mathbf{q} = 0) = I^{1\mathrm{D}} + 2 \cdot \Omega_{xy} \cdot (-0.5772 + \ln(2)) - \iint_{\mathrm{WS}} \ln(x^2+y^2)dxdy. \tag{43}$$

3.2.3 2D system

By setting the cutoff length to $z_c \equiv L_z/2$ [2], the divergences in (33) get mostly eliminated due to (39) despite of the one at the Γ-point. The cutoff potential for the 2D case is then

$$v_c^{2\mathrm{D}}(\mathbf{q}) = \frac{4\pi}{\mathbf{q}^2} \left\{ 1 - \exp(-q_{xy} z_c) \cos(q_z z_c) \right\}. \tag{44}$$

The divergence at the origin is treated in the same way as in the 1D case with the method of averaging. Here the volume $V^{2\mathrm{D}} = \frac{\Omega_{BZ}}{N_{\mathbf{k}}}$ is two-dimensional, constituting a circle centered at Γ with radius

$$\beta^{2\mathrm{D}} = \sqrt{\frac{\Omega_{BZ}}{\pi N_{\mathbf{k}}}}. \tag{45}$$

Using this, the average value for $v_c^{2\mathrm{D}}(\mathbf{q}=0)$ can be calculated. Setting $q_z = 0$ and exploiting the series expansion of the e-function to the quadratic term, which is justified because of the small values of $\beta^{2\mathrm{D}}$, one obtains

$$\begin{aligned} I^{2\mathrm{D}} &\overset{q_z=0}{=} \frac{1}{V^{2\mathrm{D}}} \int_0^{2\pi} d\varphi \int_0^{\beta^{2\mathrm{D}}} q_{xy} \frac{4\pi}{q_{xy}^2} \left\{1 - \exp(-q_{xy} z_c)\right\} dq_{xy} \\ &= \frac{8\pi^2}{V^{2\mathrm{D}}} \int_0^{\beta^{2\mathrm{D}}} \frac{1}{q_{xy}} \left\{ z_c q_{xy} - \frac{z_c^2 q_{xy}^2}{2} \right\} dq_{xy} \\ &= \frac{8\pi^2}{V^{2\mathrm{D}}} \left(\beta^{2\mathrm{D}} z_c - \frac{(z_c \beta^{2\mathrm{D}})^2}{4} \right) \\ &= 8\pi^{3/2} z_c \frac{N_{\mathbf{k}}}{\Omega_{BZ}} - 2 z_c^2 \pi. \end{aligned} \tag{46}$$

3.2.4 3D system

For completeness, the singularity of the 3D-cutoff potential at the Γ-point is also treated with the method of averaging. For this case, due to the three-dimensional Brillouin zone, $V^{3\mathrm{D}}$ represents a small sphere around Γ with radius

$$\beta^{3\mathrm{D}} = \left(\frac{3\,\Omega_{BZ}}{4\pi N_{\mathbf{k}}} \right)^{1/3}. \tag{47}$$

Thus, the averaged value for $v_c^{3\mathrm{D}}(\mathbf{q})$ is

$$I^{3\mathrm{D}} = \frac{1}{V^{3\mathrm{D}}} \int_V \frac{4\pi}{\mathbf{q}^2} d\mathbf{q} = \frac{4\pi}{V^{3\mathrm{D}}} \int d\Omega \int_0^{\beta^{3\mathrm{D}}} \frac{1}{\mathbf{q}^2} d|\mathbf{q}| = (4\pi)^{5/3} \left(\frac{9 N_{\mathbf{k}}}{\Omega_{BZ}} \right)^{2/3}. \tag{48}$$

Table 1 summarizes the results for the four different cases of dimensionality.

Table 1: *Summary of the modified expressions (to eliminate divergences) for the Coulomb-cutoff potential, calculated for every possible dimensionality, as well as the value at the* Γ*-point, determined with the method of averaging (if necessary).*

Periodicity	$v_c(\mathbf{q})$	$v_c(\mathbf{q}=0)$
0D	$\frac{4\pi}{\mathbf{q}^2}\left\{1-\cos(qR_c)\right\}$	$-2\pi R_c^2$
1D	$\iint_{\mathrm{WS}} 2\cdot \mathrm{K}_0(\lvert q_z\rvert\rho)\cdot\cos(q_x x+q_y y)\,dxdy$	$I^{\mathrm{1D}}+2\cdot\Omega_{xy}\cdot(-0.5772+\ln(2))$ $-\iint_{\mathrm{WS}}\ln(x^2+y^2)dxdy$
2D	$v_c^{\mathrm{2D}}(\mathbf{q})=\frac{4\pi}{\mathbf{q}^2}\left\{1-\exp(-q_{xy}z_c)\cos(q_z z_c)\right\}$	$8\ \pi^{3/2} z_c \frac{N_{\mathbf{k}}}{\Omega_{BZ}} - 2z_c^2\pi$
3D	$\frac{4\pi}{\mathbf{q}^2}$	$(4\pi)^{5/3}\left(\frac{9N_{\mathbf{k}}}{\Omega_{BZ}}\right)^{2/3}$

4 The exciting code and implementation details

The truncation technique presented in the previous section as well as the treatment of the singularity $\mathbf{q} \to 0$, have been implemented into the full-potential all-electron package **exciting** [5], specifically into the *GW* approximation within MBPT. The **exciting** code is able to calculate ground-state properties of a large variety of materials as well as excited-state properties *e.g.* quasiparticle band structures or optical absorption spectra. In the following short description it is sketched how **exciting** solves the KS-equation for the electronic states by using the linearized augmented plane-wave basis (LAPW), and how GWA is implemented.

4.1 The (L)APW+lo basis

In order to solve the KS-equations (12) numerically, it is necessary to introduce a basis, which is used to expand the electronic wavefunctions. For clarity, the KS-index of the wavefunction will be omitted from now on.

$$\psi_{i\mathbf{k}}(\mathbf{r}) = \sum_{\mathbf{G}} C^{\mathbf{k}}_{i\mathbf{G}} \phi_{\mathbf{G}+\mathbf{k}}(\mathbf{r}) \tag{49}$$

With a chosen basis $\phi_{\mathbf{G}+\mathbf{k}}(\mathbf{r})$, the KS-equation can be obtained in matrix-form. Equation (12) turns then into a generalized eigenvalue problem for whose solution efficient standard diagonalization techniques are applied [17]. At first sight, a plane-wave basis set seems to be a good choice, suggested by the periodic character of the wavefunction. However, it is reasonable that the electronic wavefunctions behave differently for core and valence states. The wavefunction of core states is strongly localized around the nuclei, whereas the wavefunctions of the valence states are delocalized and oscillating. Thus, a very large number of plane waves is necessary to represent the variety of electronic states accurately. The computational complexity scales with $\mathcal{O}^3(N_b)$, where N_b is the number of basis functions. Hence, the computational costs for sufficiently accurate calculations increase severely.

Observing the behavior of an electronic state, one can in principle distinguish two regions: Near by a nucleus, the electronic wavefunction resembles an atomic orbital due to the strong potential of the nucleus, whereas in the region in between, the electronic wavefunction has a delocalized character and can be well described by plane waves. Thus, it makes sense to use different functions in the two regions as already proposed by Slater [18]. Within spheres of radii R_{MT} around each nucleus α at position $\mathbf{R}_\alpha$, called muffin-tin (MT) regions, the electronic wavefunction is expanded in terms of spherical harmonics $Y_{lm}(\mathbf{r}_\alpha)$ and radial functions $u_{l\alpha}(r_\alpha)$, where $\mathbf{r}_\alpha = \mathbf{r} - \mathbf{R}_\alpha$. In the interstitial region I, plane waves are used as basis functions. This separation of the space is depicted in Fig.4. This basis is called the augmented plane-wave basis APW with basis functions

$$\phi_{\mathbf{G}+\mathbf{k}}(\mathbf{r}) = \begin{cases} \sum_{l=0}^{\infty} \sum_{m=-l}^{m} A^{\mathbf{G}+\mathbf{k}}_{lm\alpha} u_{l\alpha}(r_\alpha) Y_{lm}(\mathbf{r}_\alpha) \\ \\ \dfrac{1}{\sqrt{\Omega}} \exp[i(\mathbf{G}+\mathbf{k})\mathbf{r}] \end{cases} \tag{50}$$

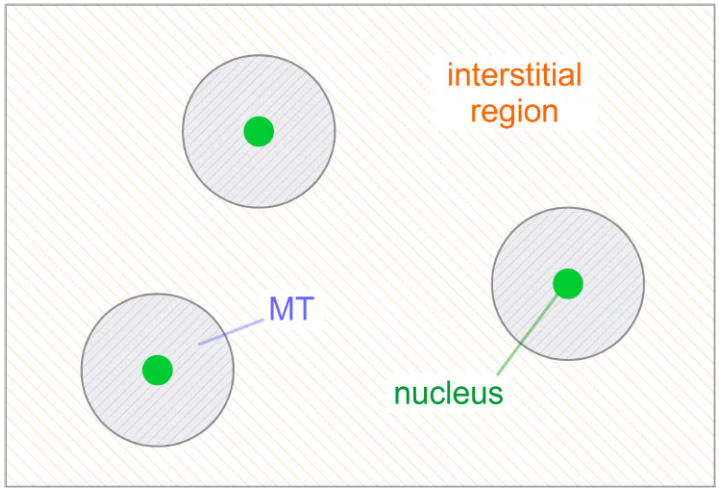

Figure 4: *Due to the different behavior of electronic wavefunctions in the vicinity of a nucleus and the interstitial region distant to the nuclei, the space is separated into two different regions where different basis function are used: the muffin-tin spheres MT (grey) around each nucleus (green) and the interstitial region (yellow).*

where Ω denotes the volume of the unit cell and $A_{lm\alpha}^{\mathbf{G}+\mathbf{k}}$ has to be chosen so that the basis functions are continuous at the sphere boundary. In the vicinity of a nucleus, also the KS-potential $V_{\mathrm{KS}}(\mathbf{r})$ is heavily influenced by the nucleus so that the radial functions $u_{l\alpha}(r)$ are constructed such to satisfy the radial Schrödinger equation with an averaged, spherically symmetric representation of the KS-potential $V_{\mathrm{MT}}(r)$

$$\left[-\frac{1}{2}\frac{d^2}{dr^2}+\frac{l(l+1)}{2r^2}+V_{\mathrm{MT}}(r)-\epsilon_{i\mathbf{k}}^{\mathrm{KS}}\right](ru_{l\alpha}(r))=0. \tag{51}$$

Thus, the radial functions depend on the KS-eigenvalue $\epsilon_{i\mathbf{k}}^{\mathrm{KS}}$. When the basis is known, the coefficients $C_{i\mathbf{G}}^{\mathbf{k}}$ and the KS-energies can be obtained by solving the eigenvalue problem

$$H^{\mathbf{k}}C^{\mathbf{k}}=\epsilon^{\mathbf{k}}S^{\mathbf{k}}C^{\mathbf{k}} \tag{52}$$

where $C^{\mathbf{k}}$ and $\epsilon^{\mathbf{k}}$ denote the coefficient and energy vector, respectively and the Hamiltonian and overlap matrix are computed as

$$H_{\mathbf{G}\mathbf{G}'}^{\mathbf{k}} = \langle\phi_{\mathbf{G}+\mathbf{k}}|-\frac{1}{2}\nabla^2+V_{\mathrm{KS}}|\phi_{\mathbf{G}'+\mathbf{k}}\rangle \tag{53}$$

$$S_{\mathbf{G}\mathbf{G}'}^{\mathbf{k}} = \langle\phi_{\mathbf{G}+\mathbf{k}}|\phi_{\mathbf{G}'+\mathbf{k}}\rangle \tag{54}$$

To make the matrices finite and the eigenvalue problem numerically computable, the plane-wave basis is made finite by defining a largest value G_{max}. Since the accuracy of a calculation not only depends on G_{max} but also on the MT-radius R_{MT}, the accuracy of the basis can be expressed through the dimensionless parameter $R_{MT}G_{max}$. It is clear that the accuracy of the calculation gets better with increasing $R_{MT}G_{max}$. But regarding the high increase of computational costs with growing $R_{MT}G_{max}$, a compromise has to be found

between the convergence speed and the accuracy of the calculation (as it is often the case in computational simulations).

The fact that the radial function is energy-dependent leads to big problems in solving the eigenvalue problem, since the basis functions and also the matrices $H^{\mathbf{k}}$ and $S^{\mathbf{k}}$ are energy dependent. Hence, Eq.(52) is not linear, and the efficient straight-forward algorithm for solving eigenvalue problems can not be applied so easily. In order to benefit yet from the fast algorithms of numerical linear algebra, a linearization of (52) in energy is necessary. A simple way to do so is to fix one energy $\epsilon_{l\alpha}$ in (51) and to use $u_{l\alpha}(r;\epsilon_{l\alpha})$ in the basis functions. It's clear that this can yield an accurate approximation for neither the wavefunction nor the actual eigenenergies ϵ. By expanding formally the radial function into a Taylor series

$$u_{l\alpha}(r;\epsilon) \approx u_{l\alpha}(r;\epsilon_{l\alpha}) + (\epsilon_{l\alpha}-\epsilon)\left.\frac{\partial u_{l\alpha}(r;\epsilon)}{\partial\epsilon}\right|_{\epsilon=\epsilon_{l\alpha}} + \frac{1}{2}(\epsilon_{l\alpha}-\epsilon)^2\left.\frac{\partial^2 u_{l\alpha}(r;\epsilon)}{\partial\epsilon^2}\right|_{\epsilon=\epsilon_{l\alpha}} + \mathcal{O}(\epsilon_{l\alpha}-\epsilon)^3 \quad (55)$$

one can see that the linearization error can be decreased by including corrections to the radial function, consisting of its derivatives. A first order correction in the spirit of a Taylor expansion leads to the linearized APW basis (LAPW), where the basis functions within the MT-parts are

$$\phi_{\mathbf{G}+\mathbf{k}}(\mathbf{r}) = \sum_{lm}\left[A^{\mathbf{G}+\mathbf{k}}_{lm\alpha}u_{l\alpha}(r_\alpha) + B^{\mathbf{G}+\mathbf{k}}_{lm\alpha}\left.\frac{\partial u_{l\alpha}(r;\epsilon)}{\partial\epsilon}\right|_{\epsilon=\epsilon_{l\alpha}}\right]Y_{lm}(\mathbf{r}_\alpha). \quad (56)$$

The coefficients $A^{\mathbf{G}+\mathbf{k}}_{lm\alpha}$ and $B^{\mathbf{G}+\mathbf{k}}_{lm\alpha}$ have to ensure continuity of the basis functions and their spacial derivatives at the MT-sphere boundary.

To improve upon LAPW and decrease the linearization error, one can take into account more corrections regarding (55) or/and define local orbitals (lo) as additional basis functions (LAPW+lo). These local orbitals are strictly zero everywhere except in one particular MT-sphere. With the introduction of lo's, the task of linearizing the secular equation is shifted from the MT-part of the APW basis functions $\phi_{\mathbf{G}+\mathbf{k}}(\mathbf{r})$ into the lo's. Hence the $\phi_{\mathbf{G}+\mathbf{k}}(\mathbf{r})$ are calculated with a frozen energy parameter for the radial functions $u_{l\alpha}(r;\epsilon_{l\alpha})$, and the local orbital within one particular MT-sphere surrounding nucleus $\mathbf{R}_{\alpha_\mu}$ can be written as

$$\phi_\mu(\mathbf{r}) = \delta_{\alpha\alpha_\mu}\delta_{ll_\mu}\delta_{mm_\mu}\left[a_\mu u_{l\alpha}(r_\alpha;\epsilon_{l\alpha}) + b_\mu\left.\frac{\partial u_{l\alpha}(r_\alpha;\epsilon)}{\partial\epsilon}\right|_{\epsilon=\epsilon_{l\alpha}}\right]Y_{lm}(\mathbf{r}_\alpha). \quad (57)$$

The coefficients a_μ and b_μ must ensure the boundary condition $\phi_\mu(|\mathbf{r}| = R_{\alpha_\mu}) = 0$ and the normalization constraint $\int_\Omega |\phi_\mu(\mathbf{r})|^2 d\mathbf{r} = 1$. Within the APW+lo basis, the electronic wavefunction is expanded in the following manner

$$\psi_{i\mathbf{k}}(\mathbf{r}) = \sum_{\mathbf{G}} C^{\mathbf{k}}_{i\mathbf{G}}\phi_{\mathbf{G}+\mathbf{k}}(\mathbf{r}) + \sum_\mu C^{\mathbf{k}}_{i\mu}\phi_\mu(\mathbf{r}) \quad (58)$$

What kind of lo's and how many of them are used to represent the wavefunction can be adjusted, depending on the required precision and the particular system.

4.2 The G_0W_0 approximation in `exciting`

A G_0W_0 calculation is based on a previous DFT calculation and uses the obtained KS-eigenfunctions $\psi_{i\mathbf{k}}(\mathbf{r})$ and eigenenergies $\epsilon_{i\mathbf{k}}$. In order to obtain the quasiparticle excitation energies (27), the non-interacting Green's function is composed of the KS-eigenfunctions

$$G_0(\mathbf{r},\mathbf{r}';\omega) = \sum_{\mathbf{k}} \left[\sum_{i}^{occ} \frac{\psi_{i\mathbf{k}}(\mathbf{r})\psi_{i\mathbf{k}}(\mathbf{r}')}{\omega - \epsilon_{i\mathbf{k}} + i\eta} + \sum_{i}^{uno} \frac{\psi_{i\mathbf{k}}(\mathbf{r})\psi_{i\mathbf{k}}(\mathbf{r}')}{\omega - \epsilon_{i\mathbf{k}} - i\eta} \right] \tag{59}$$

and hence the polarizability (24) can be expressed in the frequency domain as

$$P_0(\mathbf{r},\mathbf{r}';\omega) = \sum_{i,j} \sum_{\mathbf{k},\mathbf{k}'} F_{ij}(\mathbf{k},\mathbf{k}';\omega)\psi_{i\mathbf{k}}(\mathbf{r})\psi^*_{j\mathbf{k}-\mathbf{k}'}(\mathbf{r})\psi^*_{i\mathbf{k}}(\mathbf{r}')\psi_{j\mathbf{k}-\mathbf{k}'}(\mathbf{r}') \tag{60}$$

where F_{ij} depicts the occupation- and frequency-dependent integration weights

$$F_{ij}(\mathbf{k},\mathbf{k}';\omega) = f_{i\mathbf{k}}(1 - f_{j\mathbf{k}-\mathbf{k}'}) \cdot \left(\frac{1}{\omega - \epsilon_{j\mathbf{k}-\mathbf{k}'} + \epsilon_{i\mathbf{k}} + i\eta} - \frac{1}{\omega + \epsilon_{j\mathbf{k}-\mathbf{k}'} - \epsilon_{i\mathbf{k}} - i\eta} \right). \tag{61}$$

To transform the G_0W_0 equations (20), (21), (23), (27), (59) and (60) into matrix form, an auxiliary product basis is employed in order to expand products of KS-wavefunctions with sufficient precision.

The Coulomb potential truncation technique is used for the treatment of lower-dimensional systems. In this work, the expressions of the Coulomb-cutoff potentials in reciprocal space from Table 1 have been implemented in the equations for the dynamically-screened interaction $W(\mathbf{r},\mathbf{r}';\omega)$ (20). For the case $\mathbf{q} \to 0$, where the Coulomb-cutoff potential exhibits a singularity, the averaged values calculated in Section 3.2 have been implemented. Details regarding the implementation of the G_0W_0 in **`exciting`** can be found in Refs. 5 and 19. As a final remark, the problem of the starting-point dependence within G_0W_0 should be mentioned. Since G_0W_0 uses KS-energies and KS-eigenfunctions, the results of G_0W_0 depend on the used approximation for the exchange-correlation energy functional within the DFT calculation.

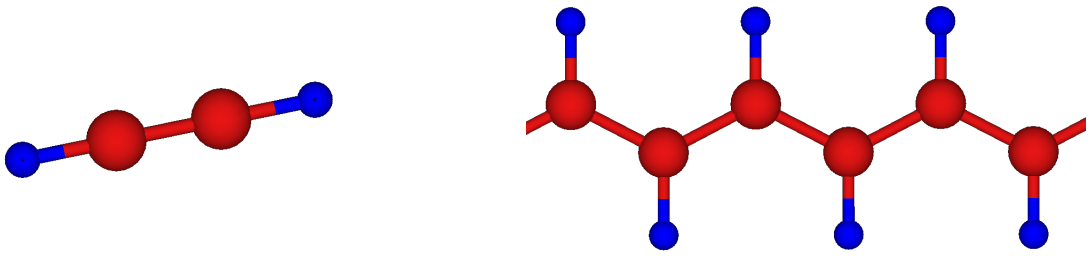

(a) *acetylene*

(b) *polyacetylene*

Figure 5: *Geometries of acetylene (left) and a polyacetylene chain (right). The systems are constituted of hydrogen (blue) and carbon (red) atoms.*

5 Results

As a test case, the implemented technique has been applied to study the electronic structure of an isolated acetylene molecule (0D system) and a polyacetylene chain (1D system). Figure 5 shows the structure of acetylene (left) and polyacetylene (right). To expand the wavefunction, an APW-lo basis has been used. All ground-state calculations were performed using LDA with an expression for the correlation-energy density from Ref. [20].

5.1 Acetylene molecule

The acetylene molecule consists of two carbon and two hydrogen atoms, where the carbon atoms create a triple bond by hybridization of an s- and an p-orbital, as shown in Figure 5. The molecular structure was obtained by a relaxation procedure, where the coordinates of the single atoms are subsequently changed in order to minimize the force between the atoms below a particularly small value. The relaxation process yielded bond distances of 2.031 a.u. between C-H and 2.281 a.u. between C-C, which is suffiently accurate in comparison with the experimental values of 2.003 a.u. and 2.273 a.u., respectively [21]. Due to the sp-hybridization of acetylene, the linearity of the molecule has already been presupposed for the relaxation process. In a 0D system, it is not meaningful to talk about a band structure, since the wavefunctions and eigenenergies do not exhibit a **k**-point dependence. The energy bands are simply horizontal and thus one rather talks about energy levels, similarly as for the hydrogen atom. Therefore, it is sufficient to sample the BZ with only one **k**-point. The cutoff parameter for the (L)APW basis has been chosen to be $R_{MT}G_{max} = 3.5$, and a local orbital (lo) for l=0 only has been used as an additional basis function. A convergence test of the E_{GS} with respect to the value of $R_{MT}G_{max}$ can be found in Appendix C (Fig.10).

Figure 6 shows the energy of the highest occupied molecular orbital (HOMO) of acetylene for different side lengths of the cubic super-cell. The calculation using G_0W_0@LDA (which means LDA was the starting point of the G_0W_0 calculation) with the implemented truncation and explicit treatment of the singularities with the method of averaging is compared to the untruncated case, where the singularities were treated by introducing an auxiliary function [22]. Using a Coulomb cutoff, a better convergence with respect to the box size can be observed. Already a boxsize of 12 a.u. yielded a converged result for E_{HOMO} where

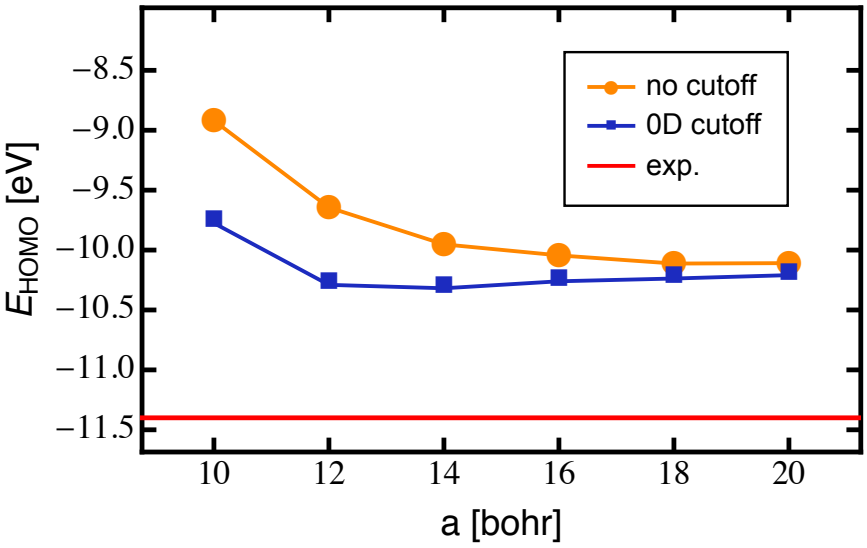

Figure 6: *Comparison of the convergence with respect to the unit cell size between the G_0W_0 calculation using the 0D cutoff and without cutoff. It can be seen that the truncation of the Coulomb potential indeed speeds up the convergence. The experimentally determined ionization energy (red) is plotted as a reference [23].*

in the case of no truncation, convergence was not reached below a boxsize of 18 a.u.. The truncation of the Coulomb potential speeds up the convergence but does not significantly affect the resulting value. Compared to the experimentally measured ionization energy $I = 11.4\,\text{eV}$ [23], the calculated value of E_{HOMO} differs by almost 10%. Calculations using a different exchange-correlation functional [24] for the ground-state calculations, which goes beyond LDA and take into account not only the local electronic density but also its spatial derivatives (generalized gradient approximation GGA), show a better agreement, *i.e.* $E_{HOMO} \approx 10.9 - 11.3\,\text{eV}$ [25], to the experimental value, but still overestimate it. One reason for this can be searched in the nonphysical self-interaction, from which not only the LDA but also the GGA suffers. The G_0W_0 is apparently not able to correct all inaccuracies made by the LDA since the G_0W_0 employs only a perturbative correction to the KS-energies.

5.2 Polyacetylene chain

As a conducting polymer, polyacetylene has already been object of interest for many different studies. One unit cell of a polyacetylene chain contains two carbon and two hydrogen atoms. A picture of the used polyacetylene structure is shown in Figure 5, which is chemically referred to as *trans*-polyacetylene. The periodic direction of the chain has been arbitrarily defined as lying along the z-axis. In order to determine the unit-cell length c in the periodic direction, a unit-cell optimization has been undertaken which yielded $c = 4.70$ a.u.. Optimization details are described in Appendix C in Figure 11. All calculations were performed on a $1 \times 1 \times 8$ **k**-point grid. The APW cutoff parameter was set to $R_{MT}G_{max} = 3.5$, and the local orbital for $l = 0$ has been additionally used. The bond lengths were determined by a structural optimization which gave a C-H bond length of 2.085 a.u. and a C-C bond length

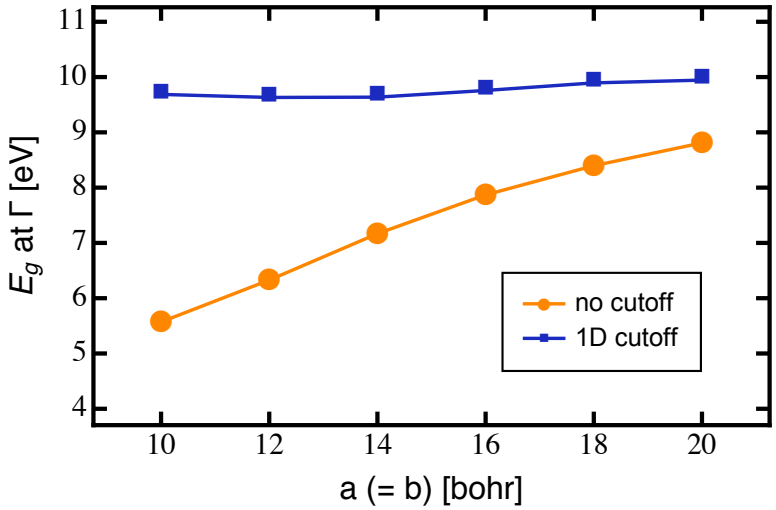

Figure 7: *The band gap for polyacetylene at the Γ-point in dependence of the box size in the finite direction. Using the Coulomb cutoff for the 1D system, the G_0W_0 calculation converges very fast in contrast to the calculation using no cutoff, which does not converge at all in the studied range of box sizes.*

of 2.649 a.u.. The angle between two C-C bonds was obtained as $\beta_{C-C} \approx 125°$.

The calculation of the band gap of polyacetylene at the Γ-point ($\mathbf{k}$-point sampling of $1 \times 1 \times 16$) with respect to the box size in the finite direction, converges much faster when a Coulomb cutoff is used. This can be seen in Figure 7, where the band-gap values for different box sizes are shown for a calculation without cutoff and with a 1D-cutoff. The effect of the truncation is vast. Without a truncation, the band-gap energy (and hence all quasiparticle energies) did not converge within the range of $10 - 20$ a.u. whereas the 1D-cutoff made converge the calculation even for a box size of 10 a.u.. This result demonstrates the large improvement that can be made regarding the computational effort when using the Coulomb truncation technique, since it allows to use much smaller box sizes.

Furthermore, the truncation of the Coulomb potential does not only increase the convergence speed of a G_0W_0 calculation with respect to the box size but also with respect to the number of $\mathbf{k}$-points, $N_\mathbf{k}$, used to sample the BZ in the infinite direction, as can be seen in Figure 8. Contrarily to the dependence on the box size in real space, the calculations without truncation do not converge at all in the reciprocal space within the investigate range of $N_\mathbf{k}$. It is interesting to mention that the convergence behavior of quasiparticle energies, calculated within the MBPT and using the cutoff potential, exhibits a very different behavior with respect to the $\mathbf{k}$-point sampling for the different dimensionalities. Contrarily to the 1D case, the convergence with respect to $N_\mathbf{k}$ worsens, when applying the Coulomb truncation in the 2D case, as can be seen in Ref. [26]. A possible explanation has to be searched in the behavior of the dielectric function in 2D, which exhibits a strong $\mathbf{q}$ dependence in the vicinity of the Γ-point. Thus, a lot of $\mathbf{k}$-points are needed to sample the BZ properly and perform integrals accurately. Why the convergence behavior in the one-dimensional case is so essentially different could be a topic of further interesting studies.

For comparison, the band gap computed by the Hartree-Fock approximation (HF) is also

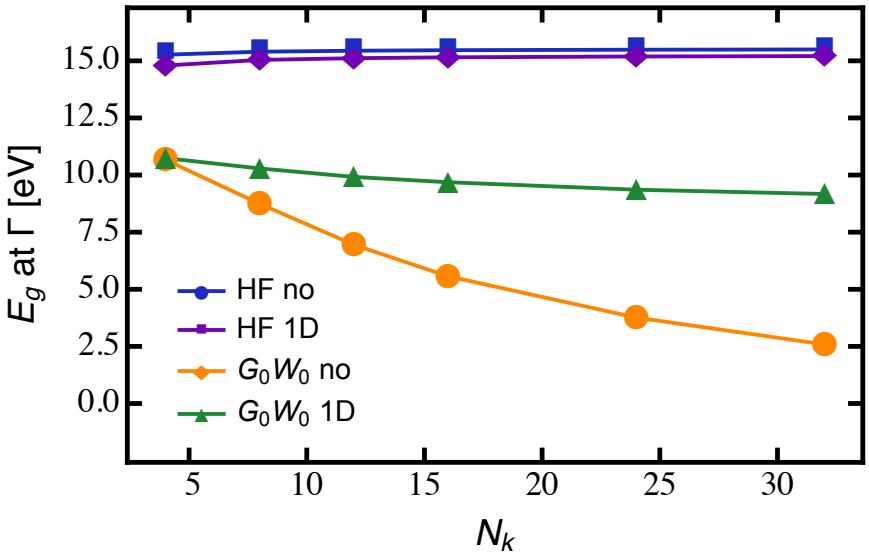

Figure 8: *The band gap for polyacetylene at the Γ-point in dependence of the number of* ***k****-points,* $N_{\mathbf{k}}$*, used to sample the BZ in the infinite direction. Comparing the calculation without cutoff (no) in contrast to the truncated case (1D), the* G_0W_0 *approach did not converge at all. The results of the calculations using the Hartree-Fock method (HF) changed only insignificantly under the application of the Coulomb potential truncation.*

depicted in Fig.8. The fact that the HF calculation is nearly not affected by the truncation shows that the dependence of the box size in G_0W_0 must come from the correlation part (at least for this system) since HF includes exact-exchange but no correlation effects into its equations. Also the correction of the G_0W_0 to the always overestimated ban-gap value calculated within the HF approach can be extracted.

The indirect band gap of polyacetylene, calculated with the truncation of the Coulomb potential at a box size of 20a.u., yielded $\approx 0.7\,\text{eV}$. Contrariwise, a phototransport experiment yielded 1.48 eV [27], and a computational approach using also Green's function theory obtained the direct band gap to be 1.86 eV [28]. One of the reasons for this underestimation in comparison with both reference values might be connected to the used bond lengths. Another one is the effect of the underlying exchange-correlation potential. Within this work, no distinction has been made between the single bond C-C and double bond C=C carbon atoms, regarding the bondlength. Experimental studies show that a bond alternation exists in real polyacetylene [29]. In addition, simulations using the tight-binding model show that bond alternation leads to a larger band gap [30]. But the main reason for the deviation of the calculated value from the two references is certainly due to errors of the DFT calculation based on LDA, which are transferred to the G_0W_0 results (starting-point dependence). Since LDA is known to underestimate band gaps, it is clear that also the G_0W_0 calculation results will be too low. The value of 1.86 eV was calculated using self-consistent GW, which lifts the starting point dependence to a certain degree and therefore produces more reliable results. The effect of the Coulomb potential on the convergence behavior is not expected to change qualitatively when including certain degrees of self-consistency into the GW approximation.

In addition, it should be mentioned that also the precise experimental determination of the band gap of polyacetylene causes large difficulties. The experimental results vary actually within a range of $1.4 - 1.8\,\mathrm{eV}$ [28], which has been assigned to *i.a.* a variation in the degree of the crystallinity of the samples.

6 Conclusions

Simulation codes exploiting 3D-periodic boundary conditions suffer from artificial-image interaction when applied to systems which are periodic in less then three dimensions. Within this work, a truncation of the Coulomb potential has been considered in order to compute and reduce the computational costs of numerical calculations with lower dimensionality. To this extent, the long-ranged Coulomb potential is cut off at a particular distance in the finite, non-periodic direction within the super-cell. As a result, lower box sizes can be used within the super-cell approach without affecting the accuracy of the computed results.

The Coulomb-cutoff potential has been summarized for all possible dimensionalities following Ref. [2]. As my own contribution, the singularity at the Γ-point of the Fourier transform of the Coulomb-cutoff potential has been treated by the method of averaging (see Table 1). This analytic treatment of the singularity reduces the number of $\mathbf{k}$-points $N_{\mathbf{k}}$ necessary to sample the BZ accurately.

The obtained results for the acetylene molecule (Figure 6) and the polyacetylene chain (8 and 7), computed with the code **exciting**, are very promising. They show an improvement of the convergence speed with respect to the super-cell size in real space. The truncation of the Coulomb potential allows for using smaller vacuum regions within a super-cell. In the case of polyacetylene, even half of the box size sufficed to gain convergent results, compared to the untruncated case. The second very interesting result is about the convergence with respect to the number of $\mathbf{k}$-points, $N_{\mathbf{k}}$. In reciprocal space, the Coulomb truncation is even necessary to produce converged results within $N_{\mathbf{k}}$s that are convenient, regarding the computational costs.

The observed deviations from experimentally and theoretically obtained reference values were explained by the inherited error from the LDA calculation, which provided the starting point for the following G_0W_0 calculation. Including self-consistency into the GW approximation [7] can cure the starting-point dependence and produces more accurate results. Nevertheless, it was not the aim of this work to reproduce exact results, but to examine the impact of the Coulomb cutoff on GW calculations. Concluding, an application of the Coulomb-cutoff potential reduces the computational costs due to the improvement of the convergence speed in real and reciprocal space. Thus, the truncation technique makes it possible to treat larger and more complicated low-dimensional systems.

7 References

1. Payne, M. C., Teter, M. P., Allan, D. C., Arias, T. A. & Joannopoulos, J. D. Iterative minimization techniques for ab initio total-energy calculations: molecular dynamics and conjugate gradients. *Rev. Mod. Phys.* **64,** 1045–1097 (1992).
2. Ismail-Beigi, S. Truncation of periodic image interactions for confined systems. *Phys. Rev. B* **73,** 233103 (2006).
3. Rozzi, C. A., Varsano, D., Marini, A., Gross, E. K. U. & Rubio, A. Exact Coulomb cutoff technique for supercell calculations. *Phys. Rev. B* **73,** 205119 (2006).
4. Jarvis, M. R., White, I. D., Godby, R. W. & Payne, M. C. Supercell technique for total-energy calculations of finite charged and polar systems. *Phys. Rev. B* **56,** 14972–14978 (1997).
5. Gulans, A. *et al.* **`exciting`**: a full-potential all-electron package implementing density-functional theory and many-body perturbation theory. *J. Phys.: Condens. Matter* **26,** 363202 (2014).
6. Cramer, C. J. *Essentials of Computational Chemistry: Theories and Models* (John Wiley & Sons, Ltd, Chichester, 2004).
7. Martin, R. M., Reining, L. & Ceperley, D. M. *Interacting Electrons: Theory and Computational Approaches* (Cambridge University Press, 2016).
8. Hohenberg, P. & Kohn, W. Inhomogeneous Electron Gas. *Phys. Rev.* **136,** B864–B871 (1964).
9. Fiolhais, C., Nogueira, F. & Marques, M. A. *A Primer in Density Functional Theory* (Springer-Verlag Berlin Heidelberg, 2003).
10. Kohn, W. & Sham, L. J. Self-Consistent Equations Including Exchange and Correlation Effects. *Phys. Rev.* **140,** A1133–A1138 (1965).
11. Ceperley, D. M. & Alder, B. J. Ground State of the Electron Gas by a Stochastic Method. *Phys. Rev. Lett.* **45,** 566–569 (1980).
12. Gunnarsson, O. & Lundqvist, B. I. Exchange and correlation in atoms, molecules, and solids by the spin-density-functional formalism. *Phys. Rev. B* **13,** 4274–4298 (1976).
13. Friedrich, C. & Schindlmayr, A. Many-Body Perturbation Theory: The GW Approximation. *NIC series* **31,** 335–355 (2006).
14. Dyson, F. J. The S Matrix in Quantum Electrodynamics. *Phys. Rev.* **75,** 1736–1755 (1949).
15. Hedin, L. New Method for Calculating the One-Particle Green's Function with Application to the Electron-Gas Problem. *Phys. Rev.* **139,** A796–A823 (1965).
16. Grosso, G. & Parravicini, G. P. *Solid State Physics* (Academic Press, Amsterdam, 2014).
17. Anderson, E. *et al. LAPACK Users' Guide* (Society for Industrial and Applied Mathematics, 1999).

18. Slater, J. C. Wave Functions in a Periodic Potential. *Phys. Rev.* **51,** 846–851 (1937).

19. Nabok, D., Gulans, A. & Draxl, C. Accurate all-electron G_0W_0 quasiparticle energies employing the full-potential augmented plane-wave method. *Phys. Rev. B* **94,** 035118 (2016).

20. Perdew, J. P. & Wang, Y. Accurate and simple analytic representation of the electron-gas correlation energy. *Phys. Rev. B* **45,** 13244–13249 (1992).

21. CRC Handbook of Chemistry and Physics, 86th Edition. *Journal of the American Chemical Society* **128,** 5585–5585 (2006).

22. Massidda, S., Posternak, M. & Baldereschi, A. Hartree-Fock LAPW approach to the electronic properties of periodic systems. *Phys. Rev. B* **48,** 5058–5068 (1993).

23. Carlier, P., Dubois, J., Masclet, P. & Mouvier, G. Spectres de photoelectrons des alcynes. *Journal of Electron Spectroscopy and Related Phenomena* **7,** 55 –67 (1975).

24. Perdew, J. P., Burke, K. & Ernzerhof, M. Generalized Gradient Approximation Made Simple. *Phys. Rev. Lett.* **77,** 3865–3868 (1996).

25. Van Setten, M. J. *et al.* GW100: Benchmarking G0W0 for Molecular Systems. *Journal of Chemical Theory and Computation* **11,** 5665–5687 (2015).

26. Rasmussen, F. A., Schmidt, P. S., Winther, K. T. & Thygesen, K. S. Efficient many-body calculations for two-dimensional materials using exact limits for the screened potential: Band gaps of $\mathbf{MoS}_2$, h-BN, and phosphorene. *Phys. Rev. B* **94,** 155406 (2016).

27. Tani, T., Grant, P., Gill, W., Street, G. & Clarke, T. Phototransport effects in polyacetylene, (CH)x. *Solid State Communications* **33,** 499 –503 (1980).

28. Ethridge, E. C., Fry, J. L. & Zaider, M. Quasiparticle spectra of trans-polyacetylene. *Phys. Rev. B* **53,** 3662–3668 (1996).

29. Yannoni, C. S. & Clarke, T. C. Molecular Geometry of cis- and trans-Polyacetylene by Nutation NMR Spectroscopy. *Phys. Rev. Lett.* **51,** 1191–1193 (1983).

30. Grant, P. & Batra, I. Band structure of polyacetylene. *Solid State Communications* **29,** 225 –229 (1979).

31. Genova, A. & Pavanello, M. Exploiting the locality of periodic subsystem density-functional theory: efficient sampling of the Brillouin zone. *Journal of Physics: Condensed Matter* **27,** 495501 (2015).

Appendix

A Bloch Theorem and k-point sampling

Due to the periodicity of the potential, the Hamiltonian is invariant under any lattice translation for the system of a crystal solid. It can be shown [16] that every state of the periodic Hamiltonian takes the form of a Bloch wave

$$\psi_{i\mathbf{k}}(\mathbf{r}) = \mathrm{e}^{i\mathbf{r}\cdot\mathbf{k}} u_{i\mathbf{k}}(\mathbf{r}) \tag{62}$$

where $u_{i,\mathbf{k}}(\mathbf{r})$ denotes a function with the same periodicity as the crystal potential. Hence, the eigenstates of a crystal Hamiltonian are labeled with the wave number $\mathbf{k}$ and the number of the energy band i. In order to take the Bloch theorem (62) within the KS-approach into account, the KS orbitals have to assume the shape of a Bloch wave as well. The total electron density can then be obtained by integrating over the full Brillouin zone (BZ) [31]

$$n(\mathbf{r}) = \frac{1}{\Omega_{BZ}} \sum_i \int f(\mathbf{k}, i) |\psi^{\mathrm{KS}}_{i\mathbf{k}}(\mathbf{r})|^2 d\mathbf{k} \tag{63}$$

where Ω_{BZ} signifies the volume of the BZ and $f(\mathbf{k}, i)$ is a continuous function of $\mathbf{k}$, denoting the occupation number of the ith energy band. In fact, the number of possible $\mathbf{k}$-vectors in each unit cell of the crystal is not infinite anymore, when imposing the Born-von Karman boundary condition. Nevertheless, (63) can still be regarded as valid due to the large number of discrete $\mathbf{k}$-vectors which lay very densely in the BZ.

In principle, the KS-orbitals have to be computed for every possible $\mathbf{k}$-point. Given that two states with near $\mathbf{k}$-vectors will differ only insignificantly, one can approximate the different states of neighboring $\mathbf{k}$-points with one wavefunction. This allows to change the integral in (63) into a finite sum over a chosen set of weighted $\mathbf{k}$-points

$$\frac{1}{\Omega_{BZ}} \int d\mathbf{k} \qquad \rightarrow \qquad \sum_{\mathbf{k}} w_{\mathbf{k}} \tag{64}$$

where $w_{\mathbf{k}}$ denotes the integration weight of a sampled $\mathbf{k}$-point. How many and which $\mathbf{k}$-points are used to sample the BZ strongly depends on the system under consideration. Metals, for instance, require a larger set of $\mathbf{k}$-points as semiconductors or insulators do for an accurate description.

B Self-consistent field cycle

The KS-equation can only be solved self-consistently since the KS-potential depends itself on the solutions of Equation (12). A self-consistent solution means that after solving (12), starting from an initial guess for the ground-state density or the KS-potential, the newly obtained density/KS-potential is used in the next iteration of solving Equation (12). Such a procedure is called pictorially a self-consistent field cycle (SCF). After every iteration the new density/KS-potential is compared with the old one and the SCF is stopped, when the difference is sufficiently small. Figure 9 shows the different steps of the SCF for a ground-state calculation in **exciting**.

The calculation of the ground-state density begins with an initial guess of the KS-potential obtained by either a superposition of atomic densities or taken from a previous DFT calculation. In order to determine the basis functions, the radial functions have to be computed by solving (51) where $\epsilon_{i\mathbf{k}}^{\mathrm{KS}}$ has been replaced by a fixed energy parameter $\epsilon_{l\alpha}$. For deep core states, it is sufficient to calculate the wavefunction by simply solving (51) with the boundary condition $u_{l\alpha}^{\mathrm{core}}(r_\alpha) \xrightarrow{r\to\infty} 0$. Within the SCF this is done before determining the basis functions. Equation (51) turns into an initial-value problem, when considering the asymptotic behavior of $u_{l\alpha}(r_\alpha)$ approaching to the nucleus. This can easily be changed into the task of solving linear algebraic equations, by introducing a grid and transforming (51) to two coupled first-order differential equations. When the basis functions are known, the matrices $H^{\mathbf{k}}$ and $S^{\mathbf{k}}$ can be calculated. The generalized eigenvalue problem (52) is then solved with standard diagonlization techniques, where the diagonalization is typically the most time-consuming part within the SCF. From the diagonalization, the eigenvalues $\epsilon_{i\mathbf{k}}$ and the eigenstates $\psi_{i\mathbf{k}}$ are obtained with which the density can be calculated

$$n(\mathbf{r}) = \sum_{\mathbf{k}} w_{\mathbf{k}} \sum_{i} f_{i\mathbf{k}} |\psi_{i\mathbf{k}}(\mathbf{r})|^2. \tag{65}$$

Then the KS-potential is updated and if no convergence has yet been reached, the next iteration is performed using the new KS-potential. In order to speed up the convergence, **exciting** mixes the initial and final KS-potential of an iteration to create the new KS-potential for the next iteration. The KS-potential, which (nearly) does not change under an iteration of the SCF, yields the electronic ground-state density of the system.

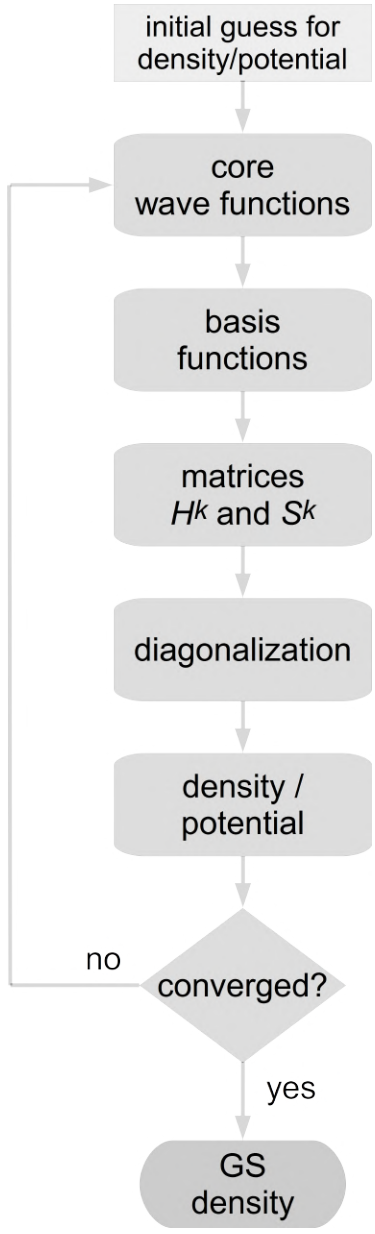

Figure 9: *The single steps of the self-consistent field cycle within the solution of the KS-equation. When the difference in the density between two iteration steps is sufficiently small, the SCF is stopped.*

C Optimization details

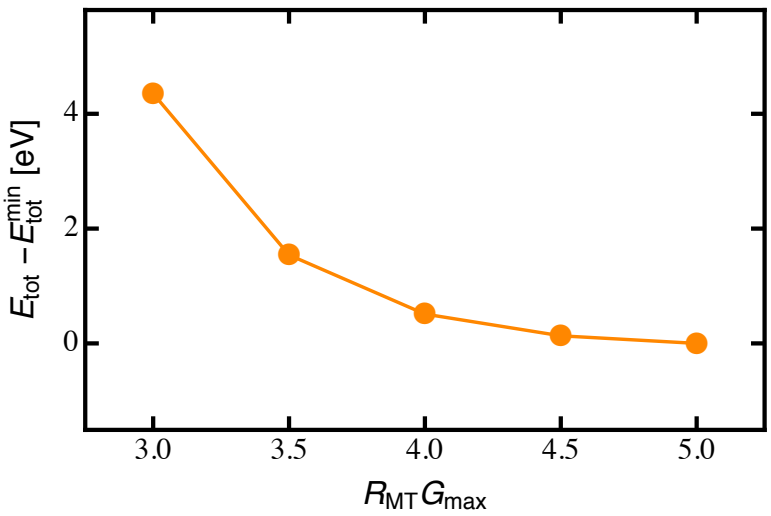

Figure 10: *Dependence of the total ground-state energy of acetylene on the basis cutoff parameter $R_{MT}G_{max}$. It's clear, that the accuracy improves with growing $R_{MT}G_{max}$ but also the computational effort increases heavily. Therefore a compromise has to be found between computational costs and accuracy of the calculation.*

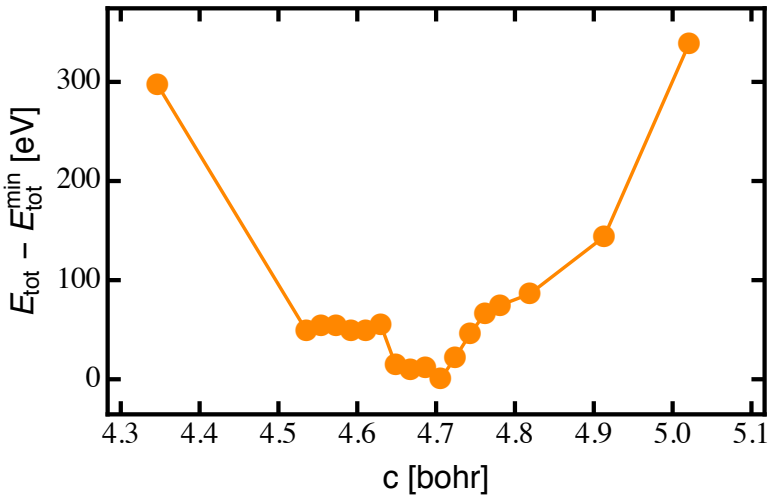

Figure 11: *Ground-state energy of a poly-acetylene chain for different box sizes in order to determine the actual lattice parameter c. $c = 4.70$ yields the lowest ground-state energy and is thus used in the further calculations. All calculations were performed with a $1 \times 1 \times 8$ BZ sampling.*

Selbstständigkeitserklärung

Ich erkläre hiermit, dass ich die vorliegende Arbeit selbstständig verfasst und noch nicht für andere Prüfungen eingereicht habe. Sämtliche Quellen einschließlich Internetquellen, die unverändert oder abgewandelt wiedergegeben werden, insbesondere Quellen für Texte, Grafiken, Tabellen und Bilder, sind als solche kenntlich gemacht. Mir ist bekannt, dass bei Verstößen gegen diese Grundsätze ein Verfahren wegen Täuschungsversuchs bzw. Täuschung eingeleitet wird.

Berlin, 8.10.18 C. W